Preprints (www.preprints.org) | NOT PEER-REVIEWED | Posted: 16 June 2020 doi:10.20944/preprints202006.0201.v1

Peer-reviewed version available at *Appl. Sci.* **2020**, *10*, 5061; doi:10.3390/app10155061

Article

Application of Post-Embedded Piezoceramic Sensors for Force Detection on RC Columns under Seismic Loading

Chiu Chien-Kuo[1]*, Wu Chia-Hsin[1], Sung Hsin-Fang[1] , Liao Wen-I[2], Lin Chih-Hsien[2]*

[1] Department of Civil and Construction Engineering, National Taiwan University of Science and Technology, Taipei 10607, Taiwan; E-mail: ckchiu@mail.ntust.edu.tw
[2] Department of Civil Engineering, National Taipei University of Technology, Taipei 10608, Taiwan; E-mail: wiliao@ntut.edu.tw
* Correspondence: ckchiu@mail.ntust.edu.tw; Tel.: +886-2-27376580, Fax: +886-2-27376606
Richman0145@gmail.com

Abstract: To quantify damage to reinforced concrete (RC) column members after an earthquake, an engineer needs to know the maximum applied force that was generated by the earthquake. Therefore, in this work, piezoceramic transducers are used to detect the applied force on an RC column member under dynamic loading. To investigate the use of post-embedded piezoceramic sensors in detecting the force that is applied to RC columns, eight full-size RC column specimens with various failure modes are tested under specific earthquake loadings. Post-embedded piezoceramic sensors are installed at a range of depths (70-80 mm) beneath the surface of a column specimen to examine the relationship between the signals that are obtained from them and the force applied by the dynamic actuator. The signals that are generated by the post-embedded piezoceramic sensors, which correlate with the applied force, are presented. These results indicate that the post-embedded piezoceramic sensors have great potential as tools for measuring the maximum applied force on an RC column in an earthquake. Restated, signals that are obtained from post-embedded piezoceramic sensors on an RC column in an earthquake can be used to determine the applied force and corresponding damage or residual seismic capacity.

Keywords: piezoceramic sensor; reinforced concrete; force; earthquake; damage.

1. Introduction

Reinforced concrete (RC) is one of the most widely used modern building materials. Natural disasters, such as earthquakes or strong ground motions, degrade RC column members. The health of a structure that includes such members must be evaluated immediately following an extreme event to provide fundamental structural information regarding building safety. Throughout the service life of a building, its structural performance must be monitored and its residual seismic or serviceability capacity must be measured. Structural health monitoring (SHM) for RC column members is part of these processes. Generally, confirmation of the safety and integrity of building structures depends on the accuracy and precision of nondestructive testing (NDT) methods, such as visual inspection (VT), acoustic emission (AE), ultrasonic testing (UT), infrared and thermal testing (IR), and others. Although NDT is practical, it has some limitations, such as the impossibility of testing a dangerous structure or one close to failure, dependence on the skills of the operator of the test instruments, and the prohibitive time required for large-scale building evaluations.

In recent decades, piezoelectric sensors have become popular SHM instruments for use in concrete buildings because of their low cost, responsiveness, active sensing, ease of use, and versatility (Liao and Jean [1]). Li et al. [2] grouped piezoelectric materials into four categories based on their structural characteristics - ceramic, single crystal, polymer and composite (combining a polymer with a single crystal or ceramic). The traditionally used piezoelectric compound is barium titanate (BaTiO3), which has been replaced by PZT and lead zirconate titanate (Pb [Zr (x) Ti (1-x)] O3), which have greater sensitivity and a higher operating temperature. An interesting phenomenon that arises from the accumulation of electric charge in certain solid materials (under applied

© 2020 by the author(s). Distributed under a Creative Commons CC BY license.

Preprints (www.preprints.org) | NOT PEER-REVIEWED | Posted: 16 June 2020 doi:10.20944/preprints202006.0201.v1

Peer-reviewed version available at Appl. Sci. 2020, 10, 5061; doi:10.3390/app10155061

mechanical stress is the reversible piezoelectricity) piezoelectric effect. When PZT ceramic is deformed, an internal measureable electric charge is generated. Conversely, the dimensions of this material are changed by applying an external electric field; and this behavior is called the inverse piezoelectric effect. Equation (1) describes the positive piezoelectric effect of a sensor and Eq. (2) describes the inverse piezo-effect of the actuator. Equations (1) and (2) are the fundamental equations for piezoelectric materials.

$$D = d^T + \varepsilon^T E \tag{1}$$

$$S = s^E T + dE \tag{2}$$

where D is the electrical displacement; d is the piezoelectric deformation constant; T is the stress field; ε^T is the dielectric permittivity; E is the electrical field; S is the strain field; and s^E is the elastic coefficient.

Gu et al. [3] studied the monitoring of the health of circular concrete columns to determine their structural performance under earthquake loading by analyzing the responses of piezoelectric ceramic transducers. Liao et al. [4] observed the structural damage status, including the degree and location of cracking damage, of in situ SHM using post-embedded piezoelectric sensors on RC bridge piers in Taiwan under reversed cyclic excitation. Chang et al. [5] investigated the effectiveness of piezoceramic transducers for monitoring structural health and developed a damage level index for multi-story RC frame structures in a shake table test. Liao and Jean [1] studied the properties of structurally damaged RC shear walls with shear failure, using the receptivity of piezoceramic transducers under reversed cyclic loading. Recently, Liao et al. [6] applied the SHM method to post-installed shear walls in an RC frame under seismic excitation, and used post-embedded piezoelectric sensors to identify surface deterioration around the boundary connections among structural elements of retrofitted walls, columns, beams and foundations. Most such uses to column members under dynamic loading have involved the monitoring of structural health using piezoelectric-based sensors. Chiu et al. [7] used pre-embedded and post-embedded piezoceramic transducers to perform crack-based damage quantification in full-size high-strength RC column specimens under cyclic loading. They found that pre-embedded piezoceramic transducers were more sensitive to maximum residual crack width than the post-embedded piezoceramic transducers, especially for shear cracks. They also found that piezoceramic transducers are not suitable for the SHM of severely damaged RC columns. The values of the damage indices that obtained using such sensors were more strongly correlated with crack width. Chiu et al. [7] introduced a normalized damage index, which they referred to as the "crack damage index", and suggested a limiting value of this damage index at each damage level. Their results revealed that the proposed piezoceramic transducer has potential for use in the SHM of an RC column.

In addition to the structural health monitoring, the piezoelectric sensors could be used for the seismic stress measurement and bond slip of steel element of the RC structure, the detection of and to detect the bolted loosening or pre-load degradation of the bolt connection etc. The entropy-based active sensing and the genetic algorithm-based least square support vector machine using PZT sensors have been developed by Wang et al. [8] for detecting the looseness of multi-bolt connections. The smart aggregates (SAs) based active sensing method was adopted by Qin et al. [9] to study the development of bond slip between the steel plate and concrete of the composite structure. Liang et al. [10] and Zeng et al. [11] also investigated the bond slip behaviors of the steel-concrete composite structures using different approaches. The piezoelectric transducer also can be utilized as energy harvesters [12-15] or passive vibration damping controller [16, 17].

For the earthquake engineering researches, it is essential to evaluate the damage states or to validate the analyzed results by monitoring the structural internal stress responses during an earthquake. The study of stress monitoring transducers for structural engineering, aerospace engineering, and robotics has drawn increasing interest from academia and industry. Hou et al. [18,

Preprints (www.preprints.org) | NOT PEER-REVIEWED | Posted: 16 June 2020 doi:10.20944/preprints202006.0201.v1

Peer-reviewed version available at Appl. Sci. 2020, 10, 5061; doi:10.3390/app10155061

19] have proposed the seismic stress sensing system by utilizing the PZT-based smart aggregates to measure the compressive seismic stress and shear stress of low to middle rise RC structures under earthquakes. The force/torque sensors using piezoelectric material for the aerospace engineering application have been developed by Li et al. [20]. Noh et al. [21] proposed a force/torque sensor based on beam theory and optoelectronic technology for robotics. Zhang et al. [22] study the influence of non-uniform stress fields on seismic stress measuring using PZT-based smart aggregates. Hou et al. [23] presented an in-built piezoelectric-based three-direction stress sensor to monitor the internal normal stresses in three directions, and the finite element analysis was performed to investigate the stress transfer inside the sensor. However, research on the internal force detection of RC structure under dynamic loadings is very scarce.

To quantify damage to an RC column member after an earthquake and to elucidate crack development in a column member, the maximum force that was applied on it as a result of the earthquake must be known. Since the measurement of maximum loading in an earthquake is difficult, in this work, piezoceramic sensors are used to quantify the force that is applied to an RC column member under dynamic loading. Piezoelectric effects are sensitive to external vibrations, and this fact can be exploited to detect the applied force in an earthquake. Post-embedded piezoceramic sensors are formed into a distributed intelligent sensor network to measure the force that is applied to an RC column member under earthquake excitation. Eight RC column specimens with three failure modes - flexural, flexural-shear and shear - are tested under dynamic loading. In the experiment, four post-embedded piezoceramic transducers are used as sensors to detect signal waves. The experimental results reveal a strong correlation between the voltage signals from piezoceramic sensors and the applied force that is induced by the dynamic actuator. Based on the experimental results, a method for estimating the maximum applied force on RC column members in an earthquake is proposed. In the future, piezoceramic transducers can be used to measure the maximum applied force on an RC column member in an earthquake and to quantify the maximum crack width following the earthquake. These two pieces of information can be combined to quantify damage and the corresponding reduction factors of strength, stiffness and energy dissipation capacity.

2. Experiment

3.1. Testing Setup

Eight sets of specimens with flexural, flexural-shear and shear failure modes are tested under dynamic seismic loading. The height of the specimens is 180 cm and their cross-sectional area is 40 × 40 cm. The actual compressive strength of concrete is 22 – 24 MPa; The main bars are SD420 of D22, and the stirrups are SD280 of D10. The specimens have the same tensile reinforcement ratio. Three stirrup ratios are used to examine the seismic reduction factors of the column specimens with three failure modes, which are flexural failure, flexural-shear failure and shear failure. Table 1 provides detailed information about each specimen.

Preprints (www.preprints.org) | NOT PEER-REVIEWED | Posted: 16 June 2020 doi:10.20944/preprints202006.0201.v1

Peer-reviewed version available at Appl. Sci. 2020, 10, 5061; doi:10.3390/app10155061

Table 1. Design details of each column specimen.

Specimen	L (cm)	Cross section (cm²)	Concrete cover (cm)	f_c' (MPa)	f_y (MPa)	f_{yt} (MPa)	S (cm)	ρ_{sh}\ (%)	Applied axial force
FF-15S-Ⅱ	180	40 × 40	4	21 (23.2*)	420	280	15	0.61	$0.1A_gf_c'$
FF-15S-Ⅲ	180	40 × 40	4	21 (22.6*)	420	280	15	0.61	$0.1A_gf_c'$
FF-15S-Ⅳ	180	40 × 40	4	21 (22.8*)	420	280	15	0.61	$0.1A_gf_c'$
FSF-15S-Ⅱ	180	40 × 40	4	21 (23.9*)	420	280	15	0.31	$0.1A_gf_c'$
FSF-15S-Ⅲ	180	40 × 40	4	21 (22.9*)	420	280	15	0.31	$0.1A_gf_c'$
FSF-15S-Ⅳ	180	40 × 40	4	21 (23.4*)	420	280	15	0.31	$0.1A_gf_c'$
SF-30S-Ⅱ	180	40 × 40	4	21 (24.4*)	420	280	30	0.15	$0.1A_gf_c'$
SF-30S-Ⅲ	180	40 × 40	4	21 (24.4*)	420	280	30	0.15	$0.1A_gf_c'$

Figure 1(a) shows that the dynamic experiment involves a reaction wall, a 50 ton dynamic actuator, and an axial force system. Before the test, a 15 cm × 15 cm grid is painted on the surface of each specimen with white cement. Using an optical measurement system, 34 markers (Fig. 1(b)) are placed on each specimen to measure the deformation in the test. Displacement gauges are set on the top and bottom of each specimen to measure the displacement of the foundation. To quantify the damage, the crack widths are measured using a microscope with a resolution of 0.01 mm. Along with the maximum crack width at a specified peak deformation, its corresponding residual crack width at an applied loading of zero is recorded. The crack type and measurement position are determined as described by Chiu et al. [7].

In the experiment, since each specimen is dynamically loaded with displacement control (Fig. 1(c)), the displacement history of each specimen is obtained from a non-linear analysis of a selected traditional low-rise street house in Taiwan. Therefore, the designed specimens are assumed to be the column members in a selected building structure. Figure 2 shows that the selected building structure has five floors with a horizontal span (four spans in total) of 17.28 m and a longitudinal span (three spans in total) of 13.68 m. The first floor is 3.6 m high, and the other floors are 3 m high. The slab thickness of each floor is 12 cm. The cross-sectional sizes of all columns, and the properties of the reinforcement and material in the structure are those of the specimens, as shown in Fig. 3. The building is located on a second-category ordinary site in Jiangjun Dist., Tainan City. Consistent with the seismic design specifications for buildings in Taiwan, the seismic demand of the building is S_{DS}=0.7 and S_{D1}=0.52, and the peak ground acceleration A_T is 0.28 g, which are consistent with a design earthquake with a returning period of 475 years.

(a)

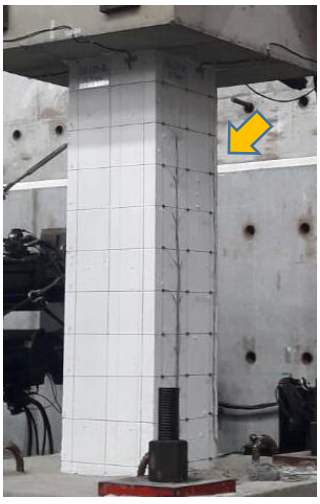

(b)

Preprints (www.preprints.org) | NOT PEER-REVIEWED | Posted: 16 June 2020 doi:10.20944/preprints202006.0201.v1

Peer-reviewed version available at Appl. Sci. 2020, 10, 5061; doi:10.3390/app10155061

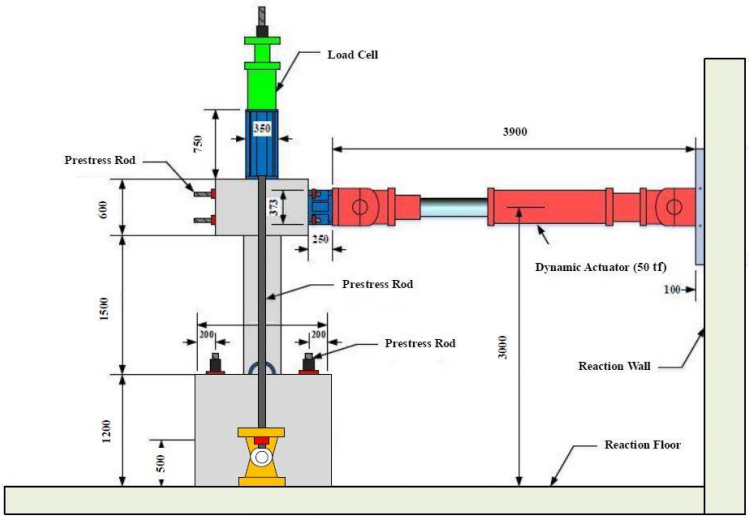

(c)

Figure 1. Experimental set up and positions of markers. (**a**) Specimen set-up; (**b**) Markers of optical measure system; (**c**) Detail of testing setup.

A piezoelectric sensor set consists of a circular piezoceramic disc, a low-frequency paired cable and a BNC connector. Table 2 presents the parameters of the circular piezoelectric transducer, which has a diameter of 20 mm and a thickness of 1 mm. The positive and negative ends of the cable must be connected carefully to the sides of a piezoceramic disc electrode and the other free ends are soldered to the BNC adapter (Fig. 4). Piezoelectric ceramics are vulnerable to moisture from fresh concrete, so they are sprayed with a thin black layer of waterproof solution. Before the non-shrinkage mortar is sealed, the piezoelectric-based sensor system is inserted into the prepared drill hole at a depth of 80 mm. Figure 5 shows the installation phases and locations of the four sensor units that are embedded in a column specimen.

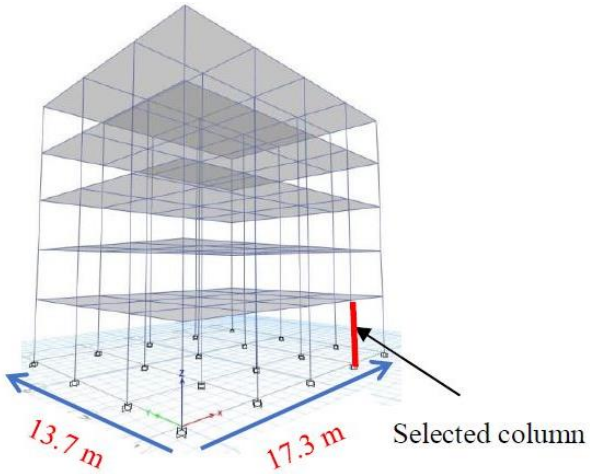

Figure 2. Finite element model and detailed information about selected building.

Preprints (www.preprints.org) | NOT PEER-REVIEWED | Posted: 16 June 2020 doi:10.20944/preprints202006.0201.v1

Peer-reviewed version available at Appl. Sci. 2020, 10, 5061; doi:10.3390/app10155061

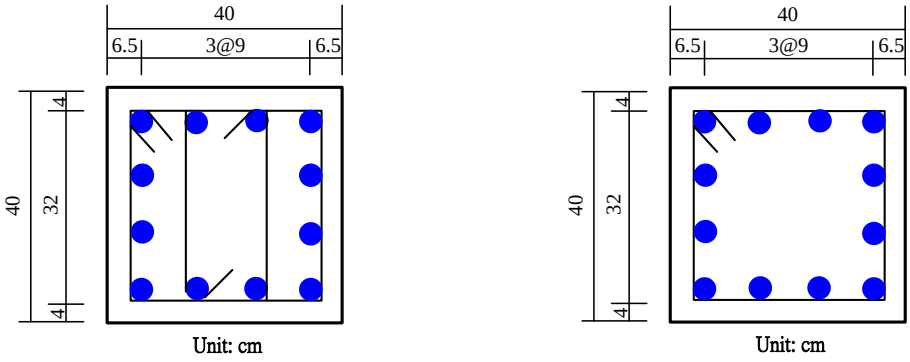

Figure 3. Detailed arrangement of reinforcement of specimen in Chiu et al. [7]. (a) FF (S = 150 mm); (b) FSF (S = 150 mm), SF (S= 300 mm).

Table 2. Properties of piezoceramic transducers.

Mass density, ϱ	Piezoelectric strain constant, d_{11}	Piezoelectric voltage constant, g_{11}	Relative permittivity, $\varepsilon_{11}^T/\varepsilon_0$	Piezoelectric coupling constant, K_{11}	Elastic constant, Y_{11}
7960 kg/m^3	345×10^{-12} m/V	9.8×10^{-3} V-m/N	3000	0.46	6.3×10^{10} N/m^2
Planar coupling factor, K_p	Piezoelectric strain constant, d_{33}	Piezoelectric voltage constant, g_{33}	Relative permittivity, $\varepsilon_{33}^T/\varepsilon_0$	Piezoelectric coupling constant, K_{33}	Elastic constant, Y_{33}
0.72	700×10^{-12} m/V	19.5×10^{-3} V-m/N	3500	0.76	5.2×10^{10} N/m^2

Figure 4. Piezoelectric sensor, drilled and post-sealed bore hole.

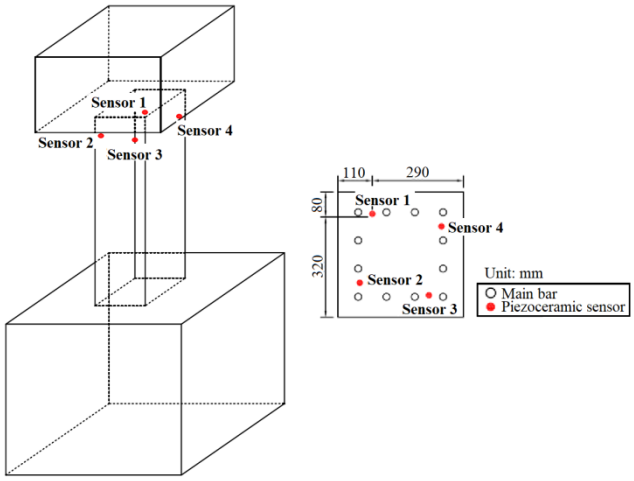

Figure 5. Locations of sensors and configuration of specimen (unit: cm).

Preprints (www.preprints.org) | NOT PEER-REVIEWED | Posted: 16 June 2020 doi:10.20944/preprints202006.0201.v1

Peer-reviewed version available at Appl. Sci. 2020, 10, 5061; doi:10.3390/app10155061

2.2. Experimental Results

For each specimen, Fig. 6 presents the input displacement signals that are obtained by structural dynamic analysis, and Fig. 7 shows the displacement signals that are measured by displacement gauges that are installed on the top part of a specimen under dynamic loading. Since Fig. 7 indicates that the measured signals are similar to the input signals, the dynamic loading control satisfies the requirements of the test. Figure 8 plots the relationship between the lateral force and the deformation of each specimen in the experiment under both dynamic and static-cyclic loading. Figure 9 presents the damage pattern of each specimen after dynamic testing.

Figure 8 and Table 3 show the initial yielding point of the reinforcement, the maximum loading point, the concrete falling point, and the final failure point of each specimen under dynamic loading, based on experimental data that were obtained using the strain gauges on the reinforcement. According to Table3, the main bars in all specimens yield under dynamic loading. In specimens FSF-15S-III, FSF-15S-IV, and SF-30S-III, the transverse reinforcement also yields under dynamic loading.

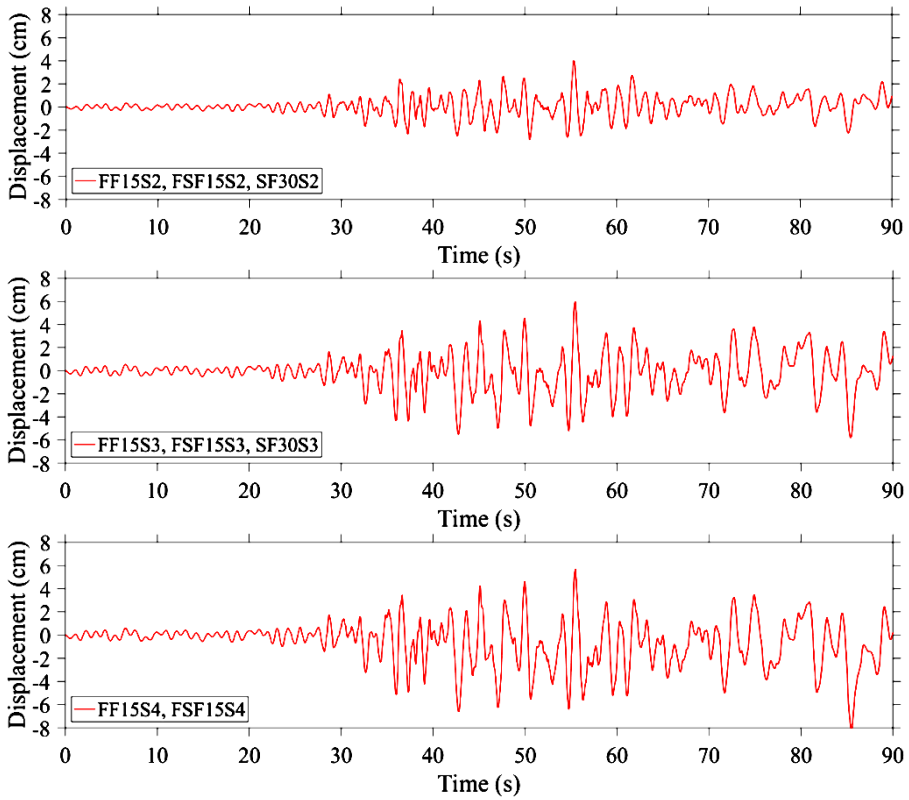

Figure 6. Seismic displacement control applied to column structures.

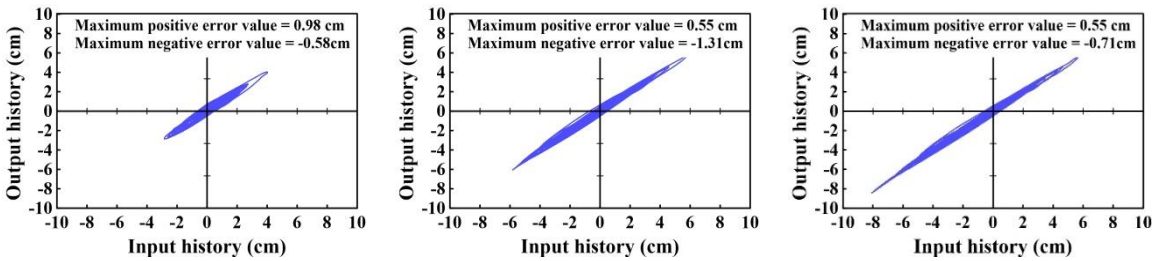

(a) (b) (c)

Figure 7. Comparison of input and output displacement histories. (a) Displacement=4cm; (b) Displacement=6cm ; (c) Displacement=8cm.

Preprints (www.preprints.org) | NOT PEER-REVIEWED | Posted: 16 June 2020 doi:10.20944/preprints202006.0201.v1

Peer-reviewed version available at Appl. Sci. 2020, 10, 5061; doi:10.3390/app10155061

Table 3. Properties of piezoceramic transducers.

Specimen	Initial yielding point of a main bar	Initial yielding point of stirrup	Maximum loading point (positive)	Maximum loading point (negative)	Concrete spalling point	Final step (strength < 60 %)
FF-15S-Ⅱ	1.0 % (Dynamic)	4.0 % (2nd)	3.0 % (1st)	-4.0 % (1st)	3.0 % (1st)	8.0 % (2nd)
FF-15S-Ⅲ	-1.0 % (Dynamic)	-4.0 % (3rd)	4.0 % (1st)	-4.0 % (1st)	3.0 % (1st)	8.0 % (1st)
FF-15S-Ⅳ	0.7 % (Dynamic)	5.5 % (1st)	4.0 % (1st)	-6.0 % (1st)	3.0 % (1st)	8.0 % (1st)
FSF-15S-Ⅱ	-1.0 % (Dynamic)	4.6 % (1st)	3.0 % (1st)	-3.0 % (1st)	3.0 % (1st)	6.0 % (2nd)
FSF-15S-Ⅲ	0.8 % (Dynamic)	-1.2 % (Dynamic)	4.0 % (1st)	-4.0 % (1st)	3.0 % (1st)	6.0 % (2nd)
FSF-15S-Ⅳ	-0.9 % (Dynamic)	-4.0 % (Dynamic)	4.0 % (1st)	-6.0 % (1st)	3.0 % (1st)	6.0 % (2nd)
SF-30S-Ⅱ	0.9 % (Dynamic)	2.6 % (3rd)	3.0 % (1st)	-3.0 % (1st)	3.0 % (1st)	4.0 % (1st)
SF-30S-Ⅲ	-0.9 % (Dynamic)	-2.6 % (Dynamic)	3.0 % (1st)	-3.0 % (1st)	3.0 % (1st)	4.0 % (1st)

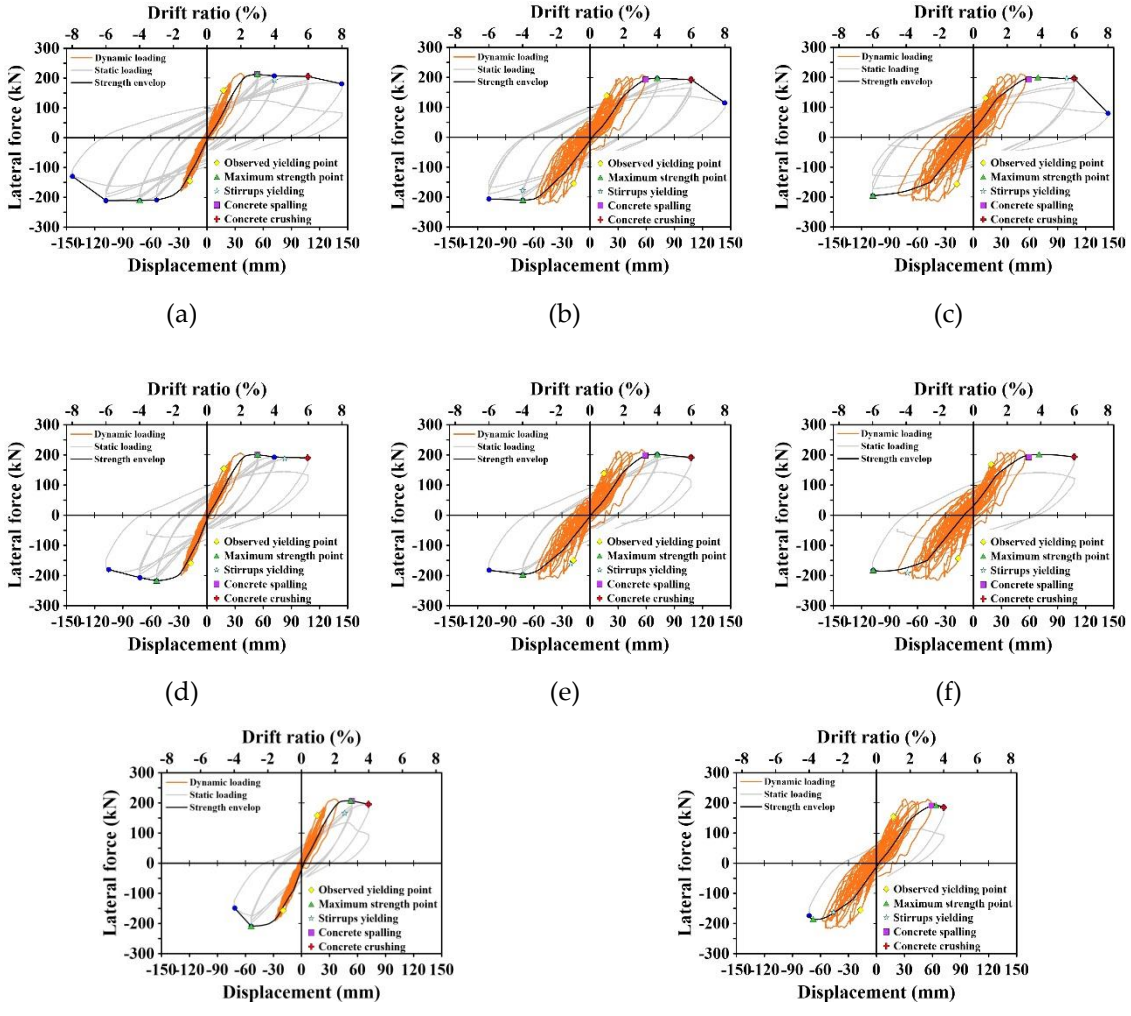

Figure 8. Relationship between lateral force and deformation of each specimen. (a) FF-15S-Ⅱ; (b) FF-15S-Ⅲ; (c) FF-15S-Ⅳ; (d) FSF-15S-Ⅱ; (e) FSF-15S-Ⅲ; (f) FSF-15S-Ⅳ; (g) SF-30S-Ⅱ; (h) SF-30S-Ⅲ.

Preprints (www.preprints.org) | NOT PEER-REVIEWED | Posted: 16 June 2020 doi:10.20944/preprints202006.0201.v1

Peer-reviewed version available at Appl. Sci. 2020, 10, 5061; doi:10.3390/app10155061

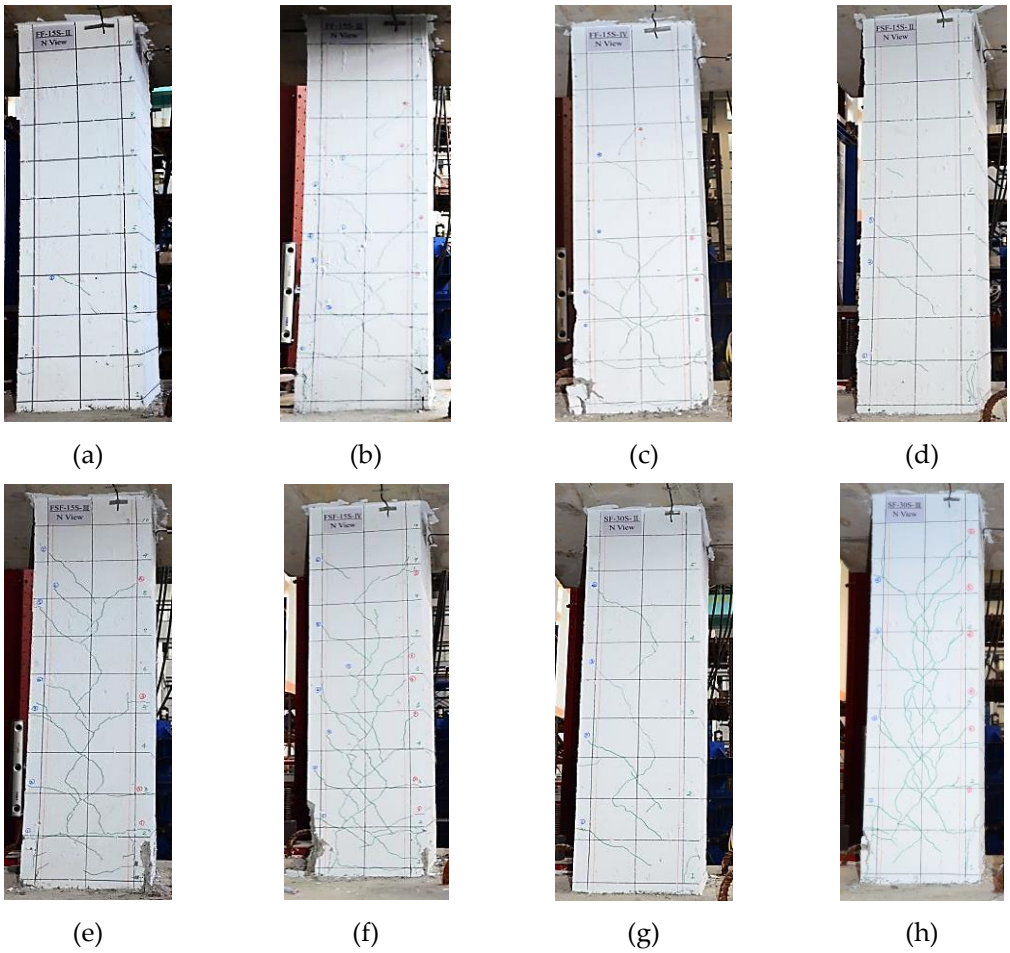

Figure 9 Damage pattern of each specimen after dynamic testing. (a) FF-15S-Ⅱ; (b) FF-15S-Ⅲ; (c) FF-15S-Ⅳ; (d) FSF-15S-Ⅱ; (e) FSF-15S-Ⅲ; (f) FSF-15S-Ⅳ; (g) SF-30S-Ⅱ; (h) SF-30S-Ⅲ.

3. Proposed Method for Detecting Force Applied to a Column Specimen in an Earthquake

3.1. Voltage Signals generated by Post-embedded Piezoceramic Sensors Under Dynamic Loading

Equation (3) is used to calculate the coefficient of correlation between the signals that are obtained using a post-embedded piezoceramic sensor and the force that is applied by the dynamic actuator ρ_F. As well as the force under dynamic testing, the coefficient of correlation between the voltage signals and the member deformation is evaluated with reference to the same equation (Eq. (3)).

$$\rho_F = \frac{\sum(s-\bar{s})\left(f-\bar{f}\right)}{\sqrt{\sum(s-\bar{s})^2\sum\left(f-\bar{f}\right)^2}} \tag{3}$$

where s and $\bar{s}$ are the voltage signal from a piezoceramic sensor and its average value, respectively; and f and $\bar{f}$ are the force applied by the dynamic actuator and its average value, respectively.

According to Table 4 and Table 5, the voltage signals that are obtained using a post-embedded piezoceramic sensor are more closely correlated with the applied force than with the applied deformation under dynamic testing. Based on these results, the following section examines the relationship between the output signals of a sensor and the applied force under dynamic testing.

Preprints (www.preprints.org) | NOT PEER-REVIEWED | Posted: 16 June 2020 doi:10.20944/preprints202006.0201.v1

Peer-reviewed version available at Appl. Sci. 2020, 10, 5061; doi:10.3390/app10155061

Table 4. Correlation coefficient between signals obtained by a post-embedded piezoceramic sensor and applied force under dynamic testing.

Specimen	FF15S2	FF15S3	FF15S4	FSF15S2	FSF15S3	FSF15S4	SF30S2	SF30S3
Sensor 1	0.72	0.49	**0.98**	0.68	0.44	0.31	0.15	**0.98**
Sensor 2	0.52	0.43	**0.95**	0.74	0.39	0.34	0.40	0.43
Sensor 3	**0.98**	**0.78**	0.36	**0.98**	**0.76**	**0.88**	**0.80**	**0.98**
Sensor 4	**0.99**	**0.77**	**0.98**	**0.99**	**0.78**	**0.88**	**0.80**	**0.99**

Table 5. Correlation coefficient between signals obtained by a post-embedded piezoceramic sensor and applied deformation under dynamic testing.

Specimen	FF15S2	FF15S3	FF15S4	FSF15S2	FSF15S3	FSF15S4	SF30S2	SF30S3
Sensor 1	0.63	0.33	**0.92**	0.60	0.36	0.20	0.05	**0.94**
Sensor 2	0.46	0.41	**0.93**	0.73	0.44	0.39	0.40	0.38
Sensor 3	**0.95**	0.66	0.40	**0.96**	**0.83**	**0.92**	**0.82**	**0.92**
Sensor 4	**0.97**	0.66	**0.93**	**0.97**	**0.84**	**0.92**	**0.82**	**0.93**

3.2. Proposed Method for Estimating Maximum Applied Force under Dynamic Loading

Table 4 provides the coefficients of correlation between the voltage signals that are obtained from a post-embedded piezoceramic sensor and the forces that are applied to a specimen under dynamic loading. According to the table, Sensor 3 and Sensor 4 are more stable than Sensor 1 and Sensor 2 because their voltage signals are not passed through and are processed by the charge amplifier. Since the charge amplifier in the test has unstable filtering functions, the correlation coefficients of Sensor 1 and Sensor 2 are smaller than those of Sensor 3 and Sensor 4. With respect to all specimens, Fig. 10 compares the signals from Sensor 3 and Sensor 4 with the applied forces. When the signals from Sensor 3 and Sensor 4 are normalized using their corresponding maximum values, their waveforms are similar to the normalized applied forces, except for specimen FF15S3. For specimens FF15S2, FSF15S2, FSF15S4 and SF30S3, since the coefficients of correlation exceed 0.9, their normalized signals vary almost exactly with the normalized applied forces. Fig. 11 presents a window view of each figure in Fig. 10 with a window size set to a period of 60 – 70 seconds. Clearly, based on Figs. 10-11 and Table 4, the post-embedded piezoceramic sensor has great potential for use in estimating the maximum force applied in an earthquake.

Based on Table 6, specimens with correlation coefficient >0.9 are used to investigate the relationship between the applied force and the voltage signal, as shown in Fig. 12. According to that figure, the relationship between the applied force and voltage signal from Sensor 4 is almost linear for each specimen. Furthermore, the regression equation for each specimen is indicated in the corresponding figure and the corresponding slopes are in the range of 357.2 – 421.1 kN/mV. Based on the average measured slope, the applied force on an RC column member in an earthquake can be estimated from the maximum voltage of the signals from the post-embedded piezoceramic sensors. Since limited experimental data were obtained in this work, the proposed method should be confirmed using more full-size specimens.

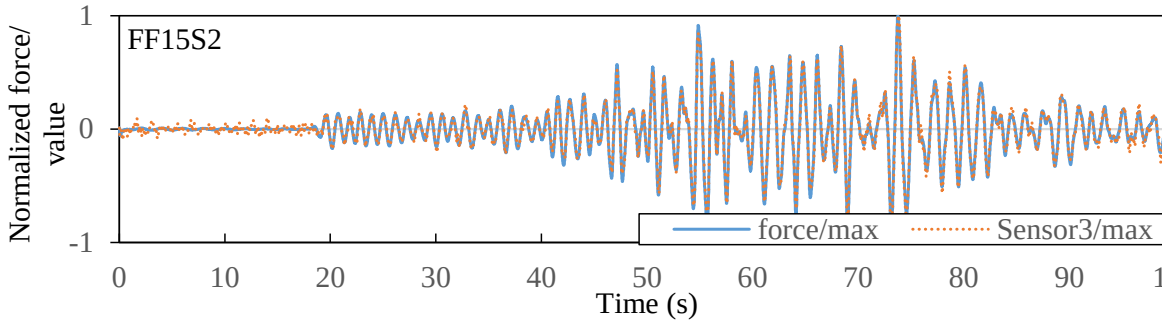

Preprints (www.preprints.org) | NOT PEER-REVIEWED | Posted: 16 June 2020 doi:10.20944/preprints202006.0201.v1

Peer-reviewed version available at Appl. Sci. 2020, 10, 5061; doi:10.3390/app10155061

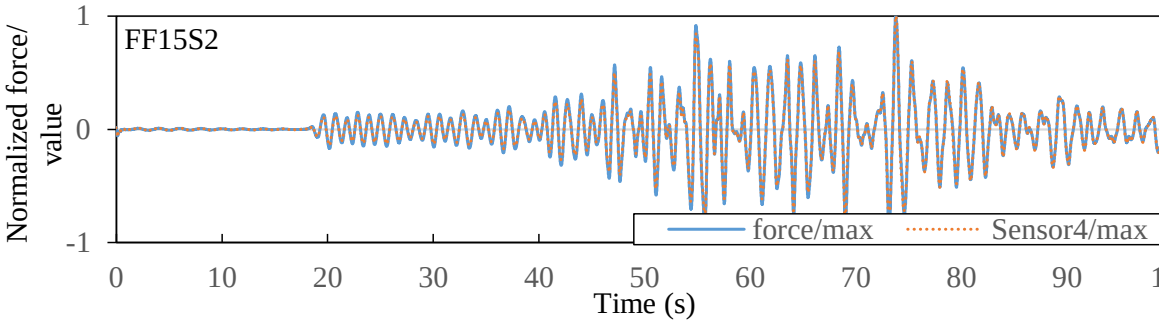

(a) FF15S2 – Sensor 3 and Sensor 4

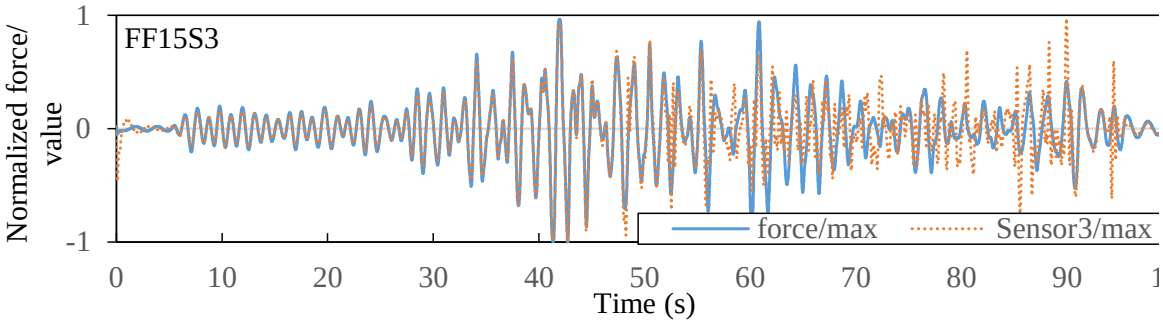

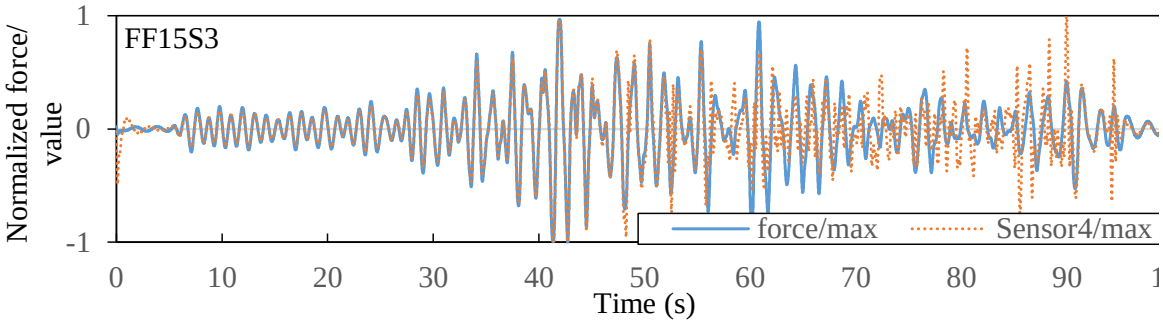

(b) FF15S3 – Sensor 3 and Sensor 4

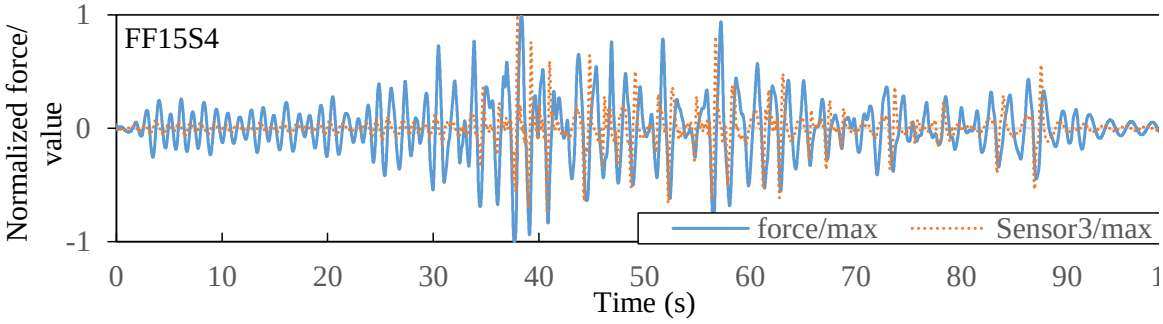

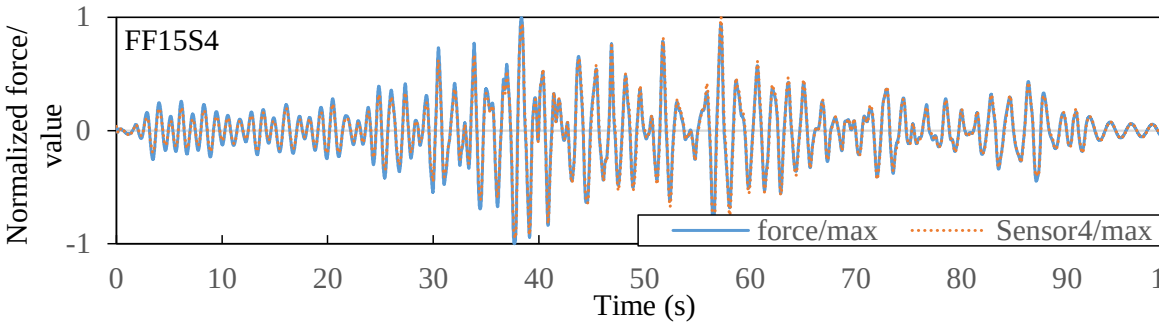

(c) FF15S4 – Sensor 3 and Sensor 4

Preprints (www.preprints.org) | NOT PEER-REVIEWED | Posted: 16 June 2020 doi:10.20944/preprints202006.0201.v1

Peer-reviewed version available at Appl. Sci. 2020, 10, 5061; doi:10.3390/app10155061

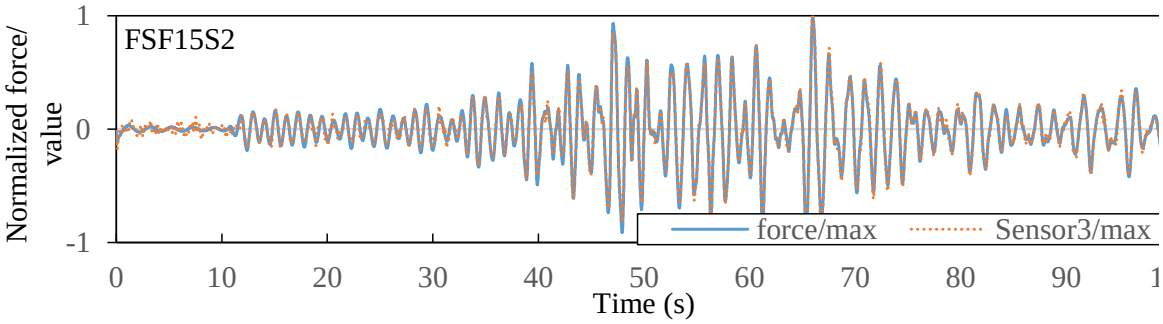

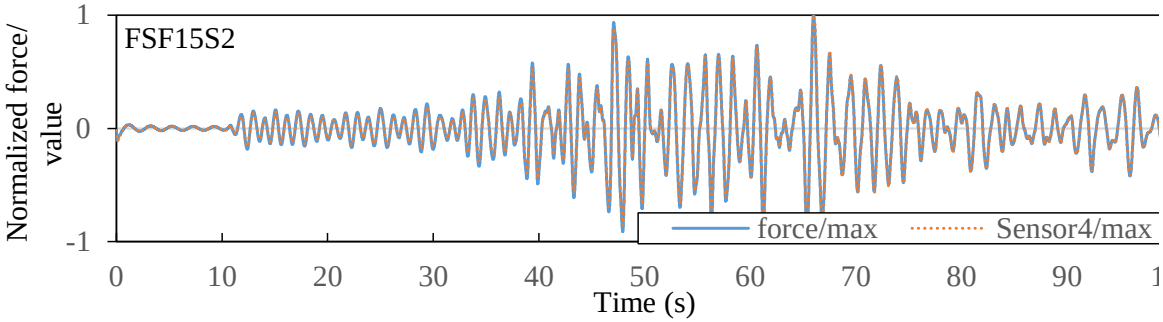

(d) FSF15S2 – Sensor 3 and Sensor 4

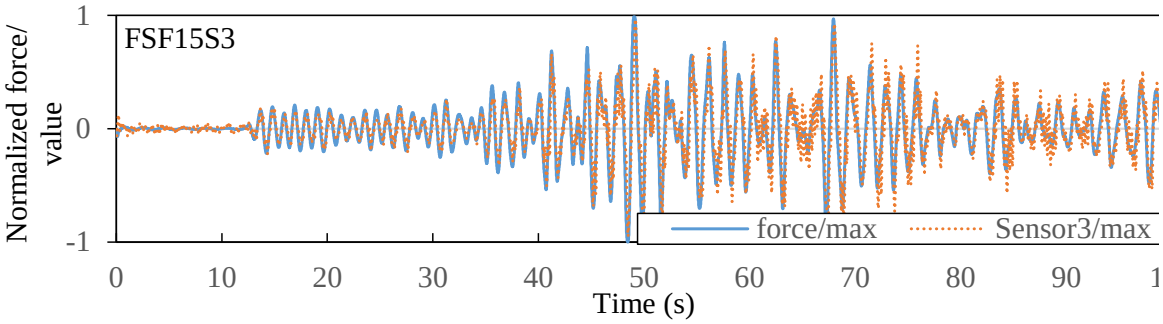

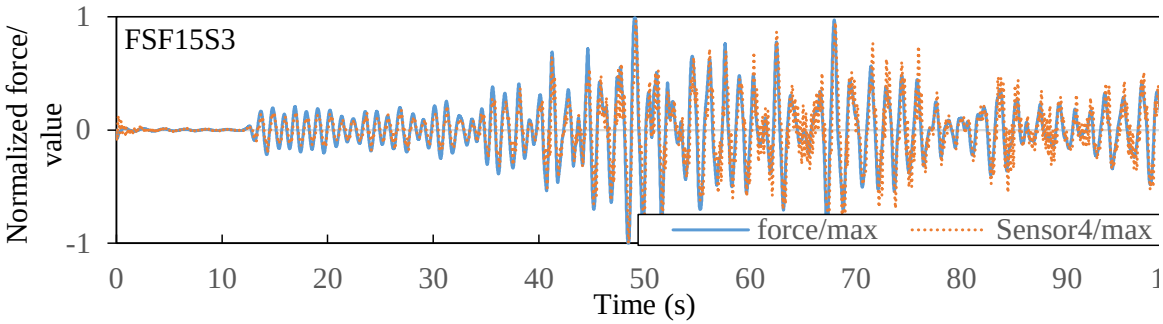

(e) FSF15S3 – Sensor 3 and Sensor 4

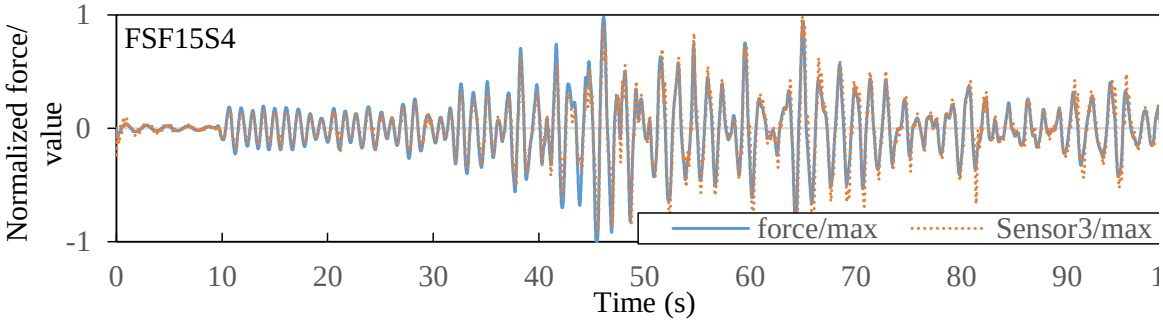

Preprints (www.preprints.org) | NOT PEER-REVIEWED | Posted: 16 June 2020 doi:10.20944/preprints202006.0201.v1

Peer-reviewed version available at Appl. Sci. 2020, 10, 5061; doi:10.3390/app10155061

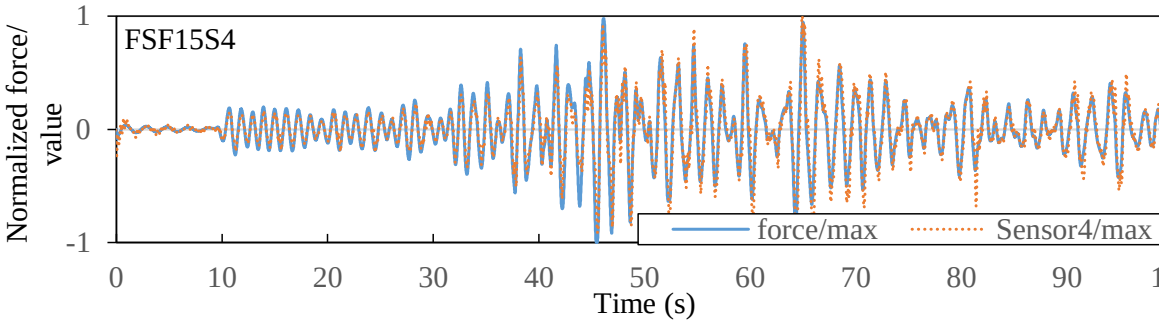

(f) FSF15S4 – Sensor 3 and Sensor 4

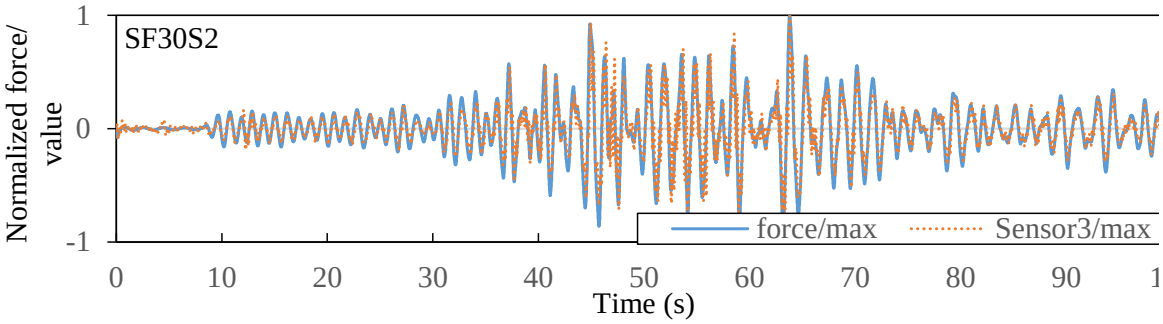

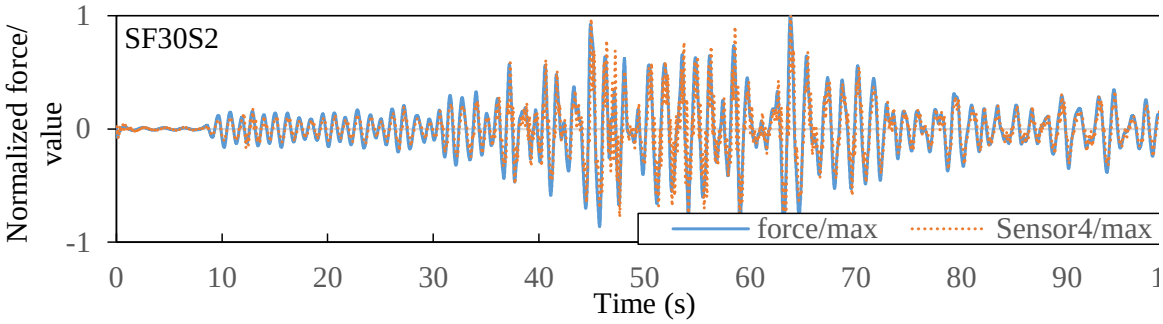

(g) SF30S2 – Sensor 3 and Sensor 4

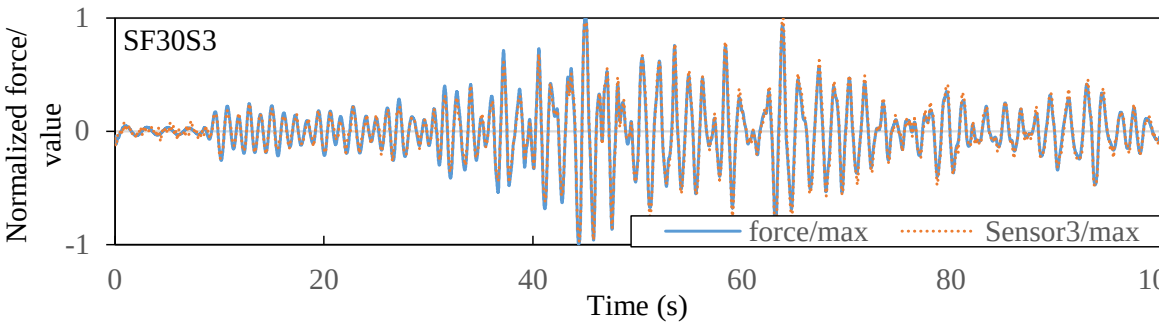

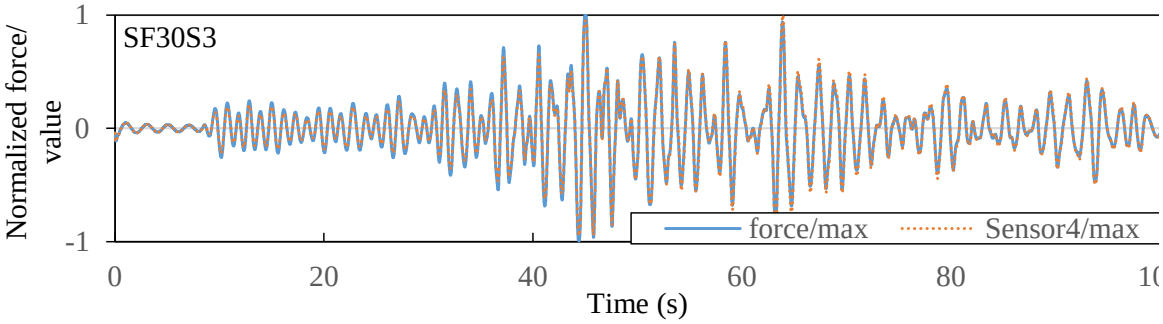

(h) SF30S3 – Sensor 3 and Sensor 4

Preprints (www.preprints.org) | NOT PEER-REVIEWED | Posted: 16 June 2020 doi:10.20944/preprints202006.0201.v1

Peer-reviewed version available at Appl. Sci. 2020, 10, 5061; doi:10.3390/app10155061

Figure 10 The waveform comparison between the sensor signals and applied force of specimens. (a) FF15S2; (b) FF15S3; (c) FF15S4; (d) FSF15S2; (e) FSF15S3; (f) FSF15S4; (g) SF30S2; (h) SF30S2.

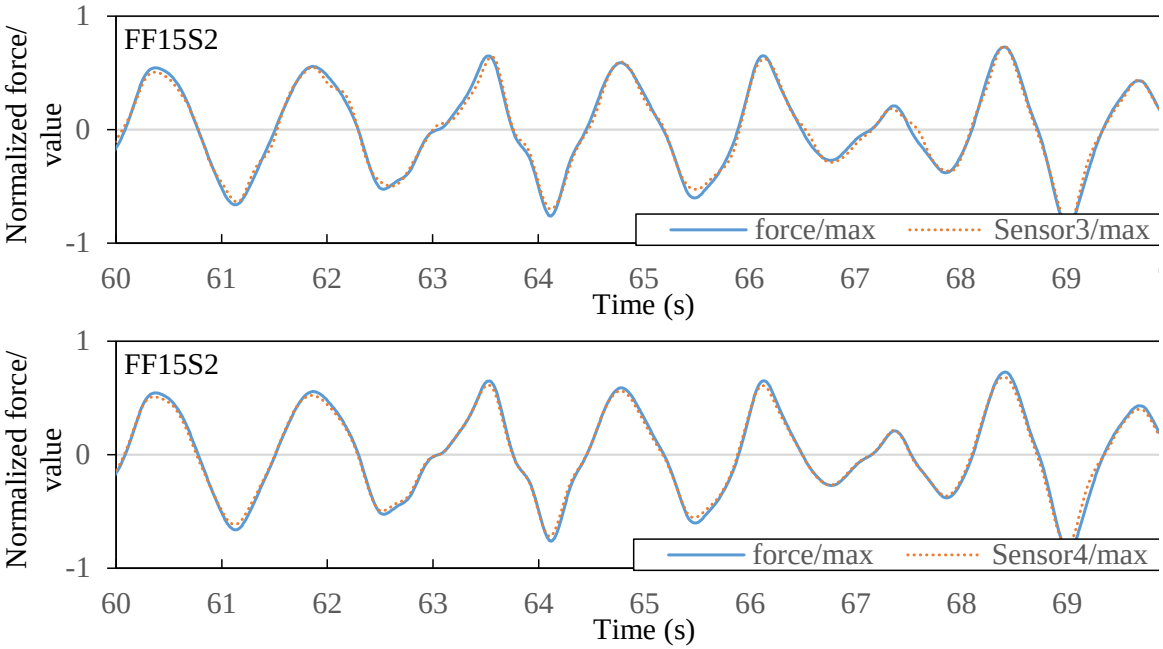

(a) FF15S2 – Sensor 3 and Sensor 4

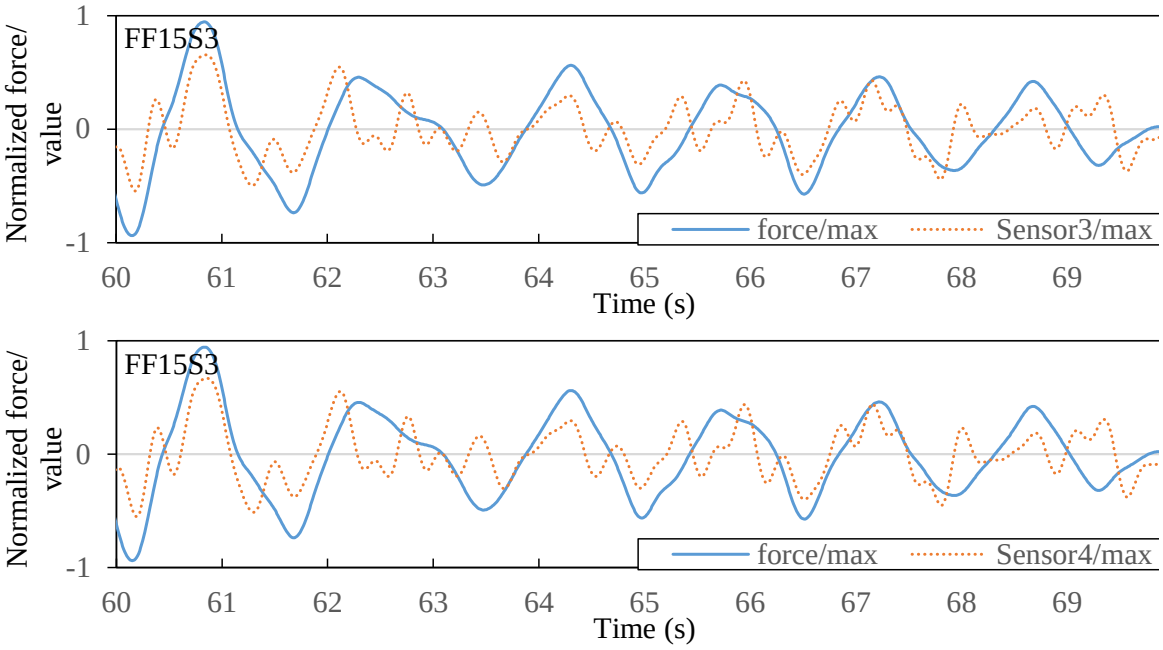

(b) FF15S3 – Sensor 3 and Sensor 4

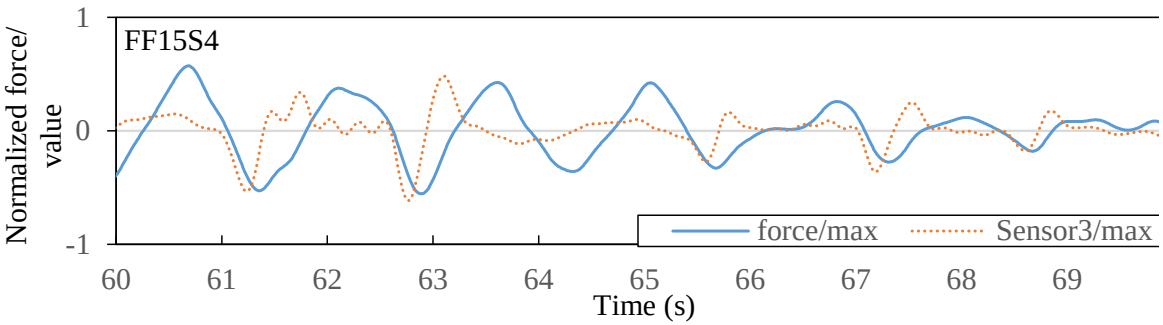

Preprints (www.preprints.org) | NOT PEER-REVIEWED | Posted: 16 June 2020 doi:10.20944/preprints202006.0201.v1

Peer-reviewed version available at Appl. Sci. 2020, 10, 5061; doi:10.3390/app10155061

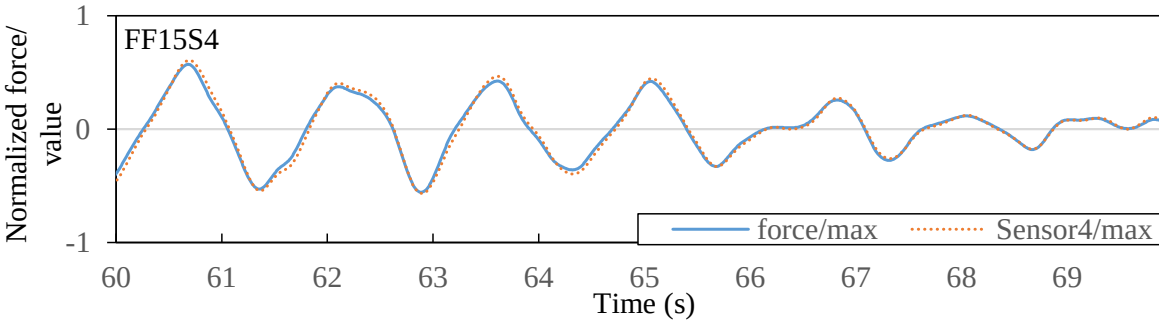

(c) FF15S4 – Sensor 3 and Sensor 4

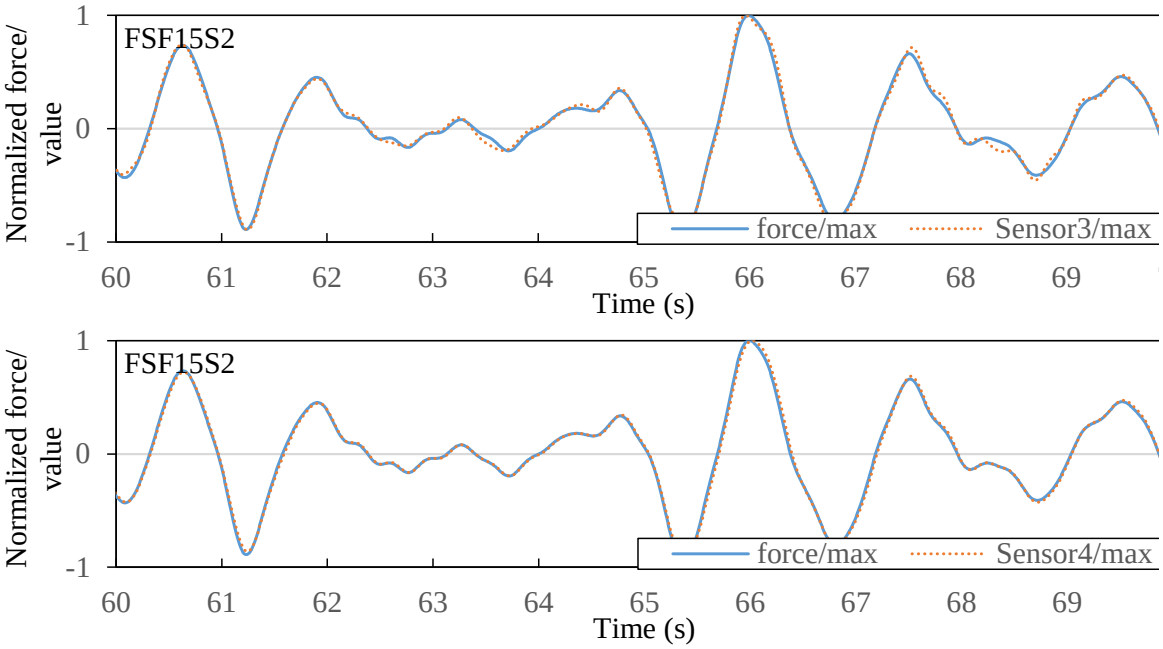

(d) FSF15S2 – Sensor 3 and Sensor 4

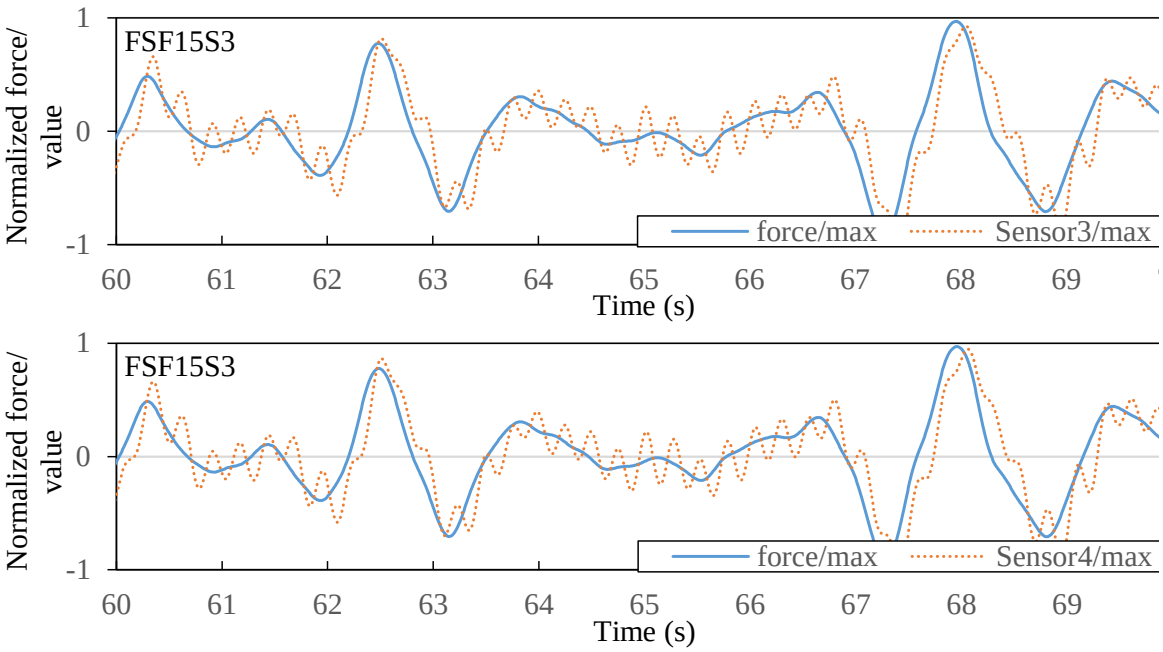

(e) FSF15S3 – Sensor 3 and Sensor 4

Preprints (www.preprints.org) | NOT PEER-REVIEWED | Posted: 16 June 2020 doi:10.20944/preprints202006.0201.v1

Peer-reviewed version available at Appl. Sci. 2020, 10, 5061; doi:10.3390/app10155061

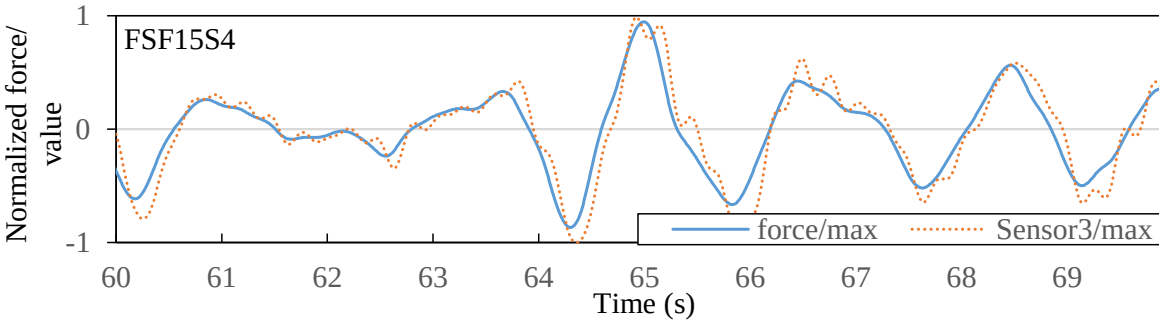

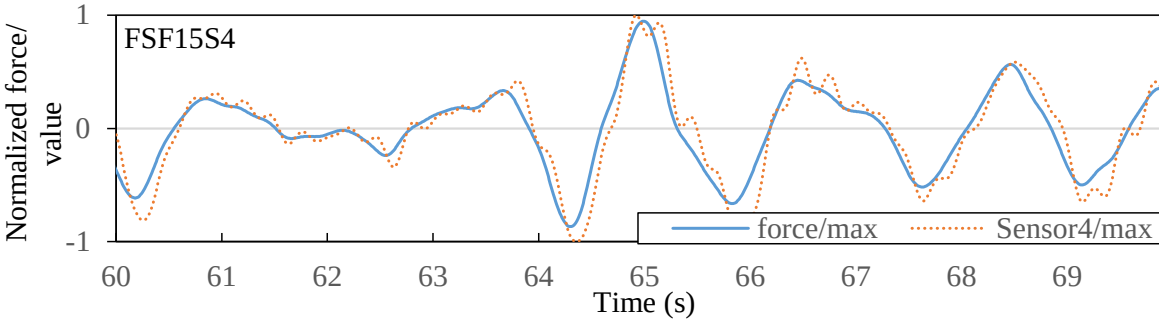

(f) FSF15S4 – Sensor 3 and Sensor 4

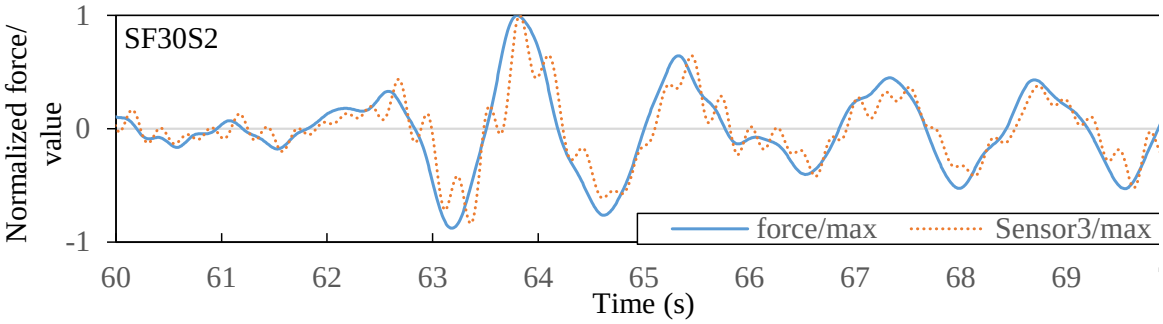

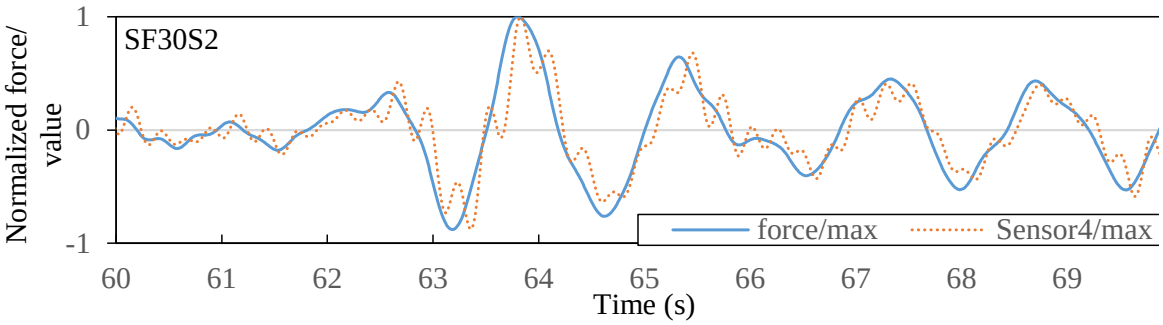

(g) SF30S2 – Sensor 3 and Sensor 4

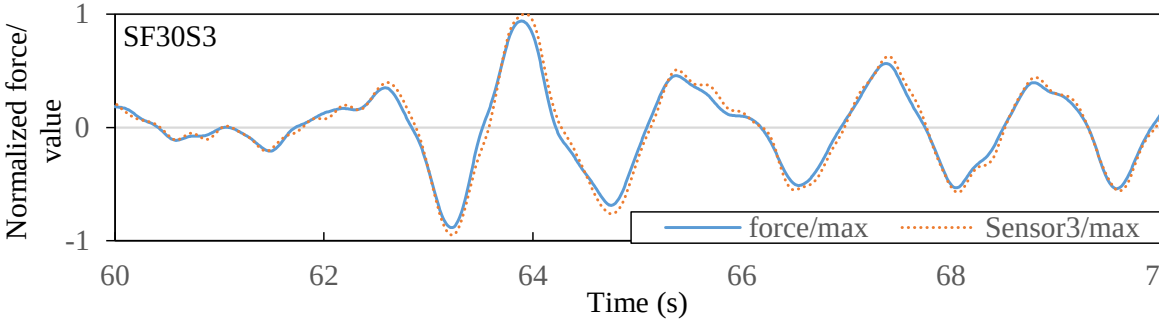

Preprints (www.preprints.org) | NOT PEER-REVIEWED | Posted: 16 June 2020 doi:10.20944/preprints202006.0201.v1

Peer-reviewed version available at Appl. Sci. 2020, 10, 5061; doi:10.3390/app10155061

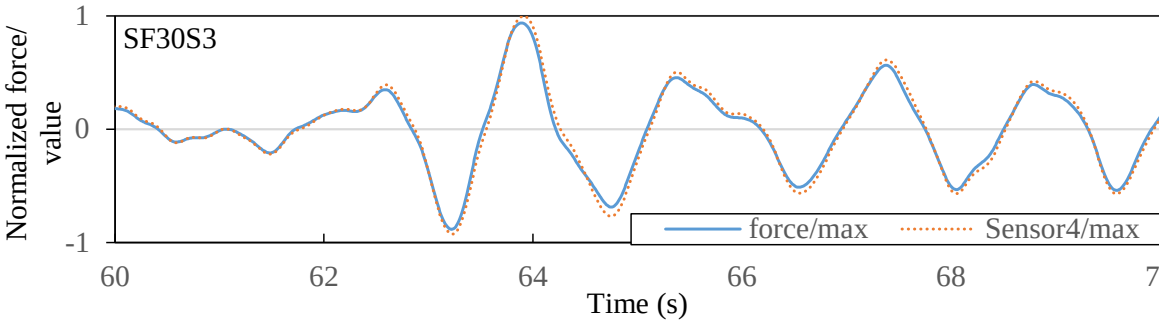

(h) SF30S3 – Sensor 3 and Sensor 4

Figure 11 Window view (60-70s) of waveforms of specimens from Fig. 3.2. (a) FF15S2; (b) FF15S3; (c) FF15S4; (d) FSF15S2; (e) FSF15S3; (f) FSF15S4; (g) SF30S2; (h) SF30S2.

Table 6. Ratio between maximum force applied to a specimen and maximum voltage signal of sensor 4.

Specimen	FF15S2	FF15S4	FSF15S2	FF15S4	SF30S2	SF30S3
F_{max}	191.69 kN	209.44 kN	193.87 kN	212.22 kN	199.31 kN	210.28 kN
$(v_{si})_{max}$	0.47 mV	0.59 mV	0.46 mV	0.83 mV	0.73 mV	0.53 mV
F_{max} / $(v_{si})_{max}$	408.25	357.27	421.05	255.32	273.51	393.09

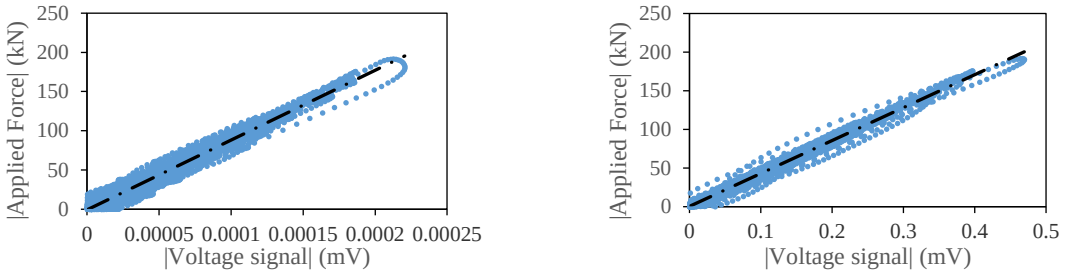

(a) FF15S2 - Sensor 3 and Sensor 4

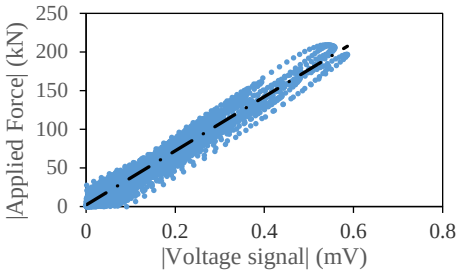

(b) FF15S4 - Sensor 4.

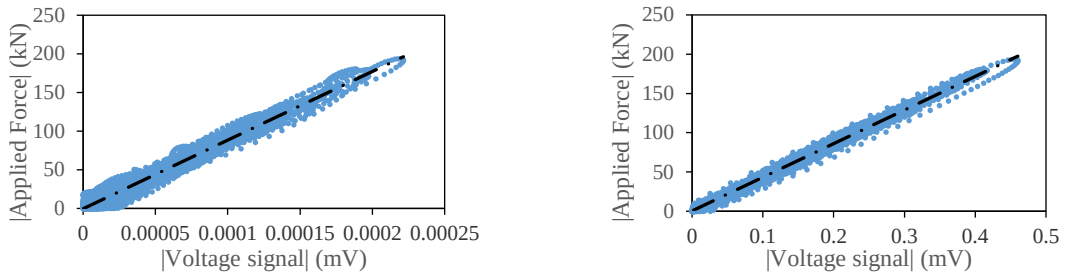

(c) FSF15S2 - Sensor 3 and Sensor 4

Preprints (www.preprints.org) | NOT PEER-REVIEWED | Posted: 16 June 2020 doi:10.20944/preprints202006.0201.v1

Peer-reviewed version available at Appl. Sci. 2020, 10, 5061; doi:10.3390/app10155061

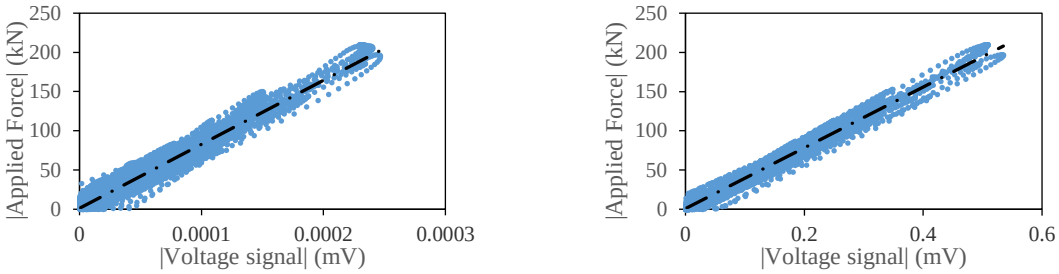

(d) SF30S3 - Sensor 3 and Sensor 4

Figure 12 Regression graphs of normalized force from specimens and normalized signal from sensors. (a) FF15S2 - Sensor 3 and Sensor 4; (b) FF15S4 - Sensor 4; (c) FSF15S2 - Sensor 3 and Sensor 4; (d) SF30S3 - Sensor 3 and Sensor 4.

4. Conclusions

This work investigates the use of post-embedded piezoceramic-based sensors to estimate the applied force on an RC column under seismic loading. Generally, in the damage-controlling design of an RC building structure, the details of the process by which each column member is damaged, including the curves of force vs. deformation, force vs. residual crack width, damage level vs. residual crack width, and damage level vs. deformation relationships, are simulated. Restated, based on the details of the damage process of a column member, post-embedded piezoceramic sensors can be used to detect the maximum force during an earthquake to quantify damage that is caused by the earthquake. The experimental results herein reveal that signal voltages that are measured by piezoceramic sensors are very strongly correlated with the forces that are applied to a specimen. Therefore, piezoceramic sensors yield the forces on a specimen during earthquake excitation. The use of piezoceramic sensors is preferred to conventional methods on account of their low cost, responsiveness, active sensing, ease of use and versatility; Post-embedded piezoceramic sensors have very great potential for practical use in estimating the maximum applied force on an RC column in an earthquake. Furthermore, based on the force-deformation relationship of such a column, its corresponding damage level can be determined from the maximum applied force, which is estimated from signals of piezoceramic sensors. In the future, piezoceramic transducers can be used to measure the maximum applied force on an RC column member in an earthquake and to determine the maximum crack width following that earthquake. Moreover, these two pieces of information can be used to determine the damage level and the corresponding reduction factors of strength, stiffness and energy dissipation capacity.

Author Contributions: Conceptualization, Chiu, C. K. and Liao, W. I.; methodology, Chiu, C. K.; software, Wu, C. H.; validation, Chiu, C. K., Liao, W. I. and Lin, C. H.; data curation, Wu, C. H. and Sung, C. F.; writing—original draft preparation, Chiu, C. K.; writing—review and editing, Liao, W. I.

Funding: This research was funded by Minister of Science and Technology (MOST), Taiwan (MOST: 107-2221-E-011 -012 -MY3).

Acknowledgments: The authors gratefully acknowledge the financial support granted by Minister of Science and Technology (MOST), Taiwan (MOST: 107-2221-E-011 -012 -MY3). The facilities for research provided by National Center for Research on Earthquake Engineering (NCREE), Taiwan, are also highly appreciated.

Conflicts of Interest: The authors declare no conflict of interest. The funders had no role in the design of the study; in the collection, analyses, or interpretation of data; in the writing of the manuscript, or in the decision to publish the results.

References

1. Liao, W. I., and Jean, W. Y. "Structural health monitoring for local damages of RC walls using piezoceramic-based sensors under seismic loading." Proc., Earth and Space 2010: Engineering, Science, Construction, and Operations in Challenging Environments, ASCE, Honolulu, Hawaii, 2017.

Preprints (www.preprints.org) | NOT PEER-REVIEWED | Posted: 16 June 2020 doi:10.20944/preprints202006.0201.v1

Peer-reviewed version available at Appl. Sci. 2020, 10, 5061; doi:10.3390/app10155061

2. Li, H., Tian, C., and Deng, Z. D. "Energy harvesting from low frequency applications using piezoelectric materials." Applied Physics Reviews, 2014; 1(4).
3. Gu, H., Moslehy, Y., Sanders, D., Song, G., and Mo, Y. L. "Multi-functional smart aggregate-based structural health monitoring of circular reinforced concrete columns subjected to seismic excitations." Smart Materials and Structures, 2010; 19(6).
4. Liao, W. I., Wang, J. X., Song, G., Gu, H., Olmi, C., Mo, Y. L., Chang, K. C., and Loh, C. H. "Structural health monitoring of concrete columns subjected to seismic excitations using piezoceramic-based sensors." Smart Materials and Structures, 2011; 20(12).
5. Chang, W., Chai, J. F., and Liao, W. I. "Structural health monitoring of a concrete frame subjected to shake table excitations using smart aggregates." Proc., Pressure Vessels & Piping Conference, ASME, Anaheim, CA, 2014.
6. Liao, W. I., Hsiao, F. P., Chiu, C. K., and Ho, C. E. "Structural health monitoring and interface damage detection for infill reinforced concrete walls in seismic retrofit of reinforced concrete frames using piezoceramic-based transducers under the cyclic loading." Applied Sciences, 2019; 9(2).
7. Chiu, C. K., Sung, H. F., Chi, K. N., Hsiao, F. P. "Experimental Quantification on the Residual Seismic Capacity of Damaged RC Column Members," International Journal of Concrete Structures and Materials,. 2019; 13:17. Available at https://doi.org/10.1186/s40069-019-0338-z.
8. Wang, F., Chen, Z., & Song, G. "Monitoring of multi-bolt connection looseness using entropy-based active sensing and genetic algorithm-based least square support vector machine." Mechanical Systems and Signal Processing, 2020; 136, 106507.
9. Qin, F.; Kong, Q.; Li, M.; Mo, Y. L.; Song, G.; Fan, F., Bond slip detection of steel plate and concrete beams using smart aggregates. Smart Materials and Structures, 2015, 24, (11), 115039.
10. Liang, Y.; Li, D.; Parvasi, S. M.; Kong, Q.; Lim, I.; Song, G., Bond-slip detection of concrete-encased composite structure using electro-mechanical impedance technique. Smart Material and Structures 2016, 25, 904 (9), 095003.
11. Zeng, L.; Parvasi, S. M.; Kong, Q.; Huo, L.; Lim, I.; Li, M.; Song, G., Bond slip detection of concrete-encased composite structure using shear wave based active sensing approach. Smart Materials and Structures 2015, 24, (12), 125026.
12. Guyomar, D.; Badel, A.; Lefeuvre, E.; Richard, C., Toward energy harvesting using active materials and conversion improvement by nonlinear processing. IEEE Transactions on Ultrasonics Ferroelectrics and Frequency Control 2005, 52, (4), 584-595.
13. Wang, G., Analysis of bimorph piezoelectric beam energy harvesters using Timoshenko and Euler-Bernoulli beam theory. Journal of Intelligent Material Systems and Structures 2013, 24, (2), 226-239.
14. Lefeuvre, E.; Badel, A.; Richard, C.; Petit, L.; Guyomar, D., A comparison between several vibration-powered piezoelectric generators for standalone systems. Sensors & Actuators A Physical 2009, 126, (2), 405-416.
15. Yan, B.; Zhang, S. W.; Zhang, X. N.; Wang, K.; Wu, C. Y., Self-powered electromagnetic energy harvesting for the low power consumption electronics: Design and experiment. Int. J. Appl. Electromagn. Mech. 2017, 54, (2), 165-175.
16. Corr, L. R.; Clark, W. W., A Novel SemiActive Multi-Modal Vibration Control Law for a Piezoceramic Actuator. Journal of Vibration and Acoustics 2003, 125, (2), 214-222.
17. Niederberger, D.; Fleming, A.; Moheimani, S. O. R.; Morari, M., Adaptive multi-mode resonant piezoelectric shunt damping. Smart Materials & Structures 2004, 13, (5), 1025.
18. Hou, S, Zhang, H.B., and Ou, J.P., A PZT-based smart aggregate for compressive seismic stress monitoring, Smart Materials and Structures 2012, 21(10):105035.
19. Hou, S, Zhang H.B., Ou J.P., A PZT-based smart aggregate for seismic shear stress monitoring. Smart Materials and Structures 2013, 22:65012.
20. Li, Y,, Wang, G,, Yang, X,, Research on static decoupling algorithm for piezoelectric six axis force/torque sensor based on LSSVR fusion algorithm., Mechanical Systems and Signal Processing 2018, 110: 509–520.
21. Noh, Y., Bimbo, J., Sareh S., Multi-axis force/torque sensor based on simply-supported beam and optoelectro- nics. Sensors 2016, 16: 1936.
22. Zhang, H.B., Hou, S, and Ou, J.P., SA-based concrete seismic stress monitoring: The influence of non-uniform stress fields, Engineering Structures 2019, 190, 66-75.
23. Hou, S., Cui, L.L., and Xibing Xu, X.B., A piezoelectric-based three-direction normal stress sensor for concrete structures, Journal of Intelligent Material Systems and Structures 2019, 30(12), 1858–1867.